
Article:
Hunt, Neil Terrence orcid.org/0000-0001-7400-5152 (2022) Reversible Glutamate Coordination to High-Valent Nickel Protects the Active Site of a [NiFe] Hydrogenase from Oxygen. Journal of the American Chemical Society. 17022−17032. ISSN 1520-5126

https://doi.org/10.1021/jacs.2c06400

Reversible glutamate coordination to high-valent nickel protects the active site of a [NiFe] hydrogenase from oxygen

Catharina J. Kulka-Peschke[a‡], Anne-Christine Schulz[a‡], Christian Lorent[a‡], Yvonne Rippers[b], Stefan Wahlefeld[a], Janina Preissler[a], Claudia Schulz[a], Charlotte Wiemann[a], Cornelius C. M. Bernitzky[b], Chara Karafoulidi-Retsou[a], Solomon L. D. Wrathall[c], Barbara Procacci[c], Hiroaki Matsuura[d], Gregory M. Greetham[e], Christian Teutloff[b], Lars Lauterbach[f], Yoshiki Higuchi[g], Masaharu Ishii[h], Neil T. Hunt[c], Oliver Lenz[a]*, Ingo Zebger[a]*, Marius Horch[b]*

[a] Institut für Chemie, Sekr. PC14, Technische Universität Berlin, Straße des 17. Juni 135, D-10623 Berlin, Germany

[b] Fachbereich Physik, Freie Universität Berlin, Arnimallee 14, D-14195 Berlin, Germany

[c] Department of Chemistry & York Biomedical Research Institute, University of York, Heslington, York, YO10 5DD, United Kingdom

[d] Life Science Research Infrastructure Group, RIKEN/SPring-8 Center, 1-1-1 Kouto, Sayo-cho, Sayo-gun, Hyogo 679-5148, Japan

[e] STFC Central Laser Facility, Research Complex at Harwell, Rutherford Appleton Laboratory, Harwell Science and Innovation Campus, Didcot, Oxford, OX11 0QX, United Kingdom

[f] Institute of Applied Microbiology, Synthetic Microbiology, RWTH Aachen University, Worringer Weg 1, D-52074 Aachen, Germany

[g] Graduate School of Science, University of Hyogo, 3-2-1 Koto, Kamigori-cho, Ako-gun, Hyogo 678-1297, Japan

[h] Graduate School of Agricultural and Life Sciences / Faculty of Agriculture, The University of Tokyo, 1-1-1, Yayoi, Bunkyo-ku, Tokyo 113-8657, Japan

KEYWORDS: Biohydrogen, Hydrogenase, Oxygen Protection, Thermostable Enzymes, Spectroscopy, 2D-IR Spectroscopy

ABSTRACT: NAD^+-reducing [NiFe] hydrogenases are valuable biocatalysts for H_2-based energy conversion and the regeneration of nucleotide cofactors. While most hydrogenases are sensitive towards O_2 and elevated temperatures, the soluble NAD^+-reducing [NiFe] hydrogenase from *Hydrogenophilus thermoluteolus* (*Ht*SH) is O_2-tolerant and thermostable. Thus, it represents a promising candidate for biotechnological applications. Here, we have investigated the catalytic activity and active-site structure of native *Ht*SH and variants in which a glutamate residue in the active site cavity was replaced by glutamine, alanine, and aspartate. Our biochemical, spectroscopic, and theoretical studies reveal that at least two active-site states of oxidized *Ht*SH feature an unusual architecture in which the glutamate acts as a terminal ligand of the active-site nickel. This observation demonstrates that crystallographically observed glutamate coordination represents a native feature of the enzyme. One of these states is diamagnetic and characterized by a very high stretching frequency of an iron-bound active-site CO ligand. Supported by density-functional-theory calculations, we identify this state as a high-valent species with a biologically unprecedented formal Ni(IV) ground state. Detailed insights into its structure and dynamics were obtained by ultrafast and two-dimensional infrared spectroscopy, demonstrating that it represents a conformationally strained state with unusual bond properties. Our data further show that this state is selectively and reversibly formed under oxic conditions, especially upon rapid exposure to high O_2 levels. We conclude that the kinetically controlled formation of this six-coordinate high-valent state represents a specific and precisely orchestrated stereoelectronic response towards O_2 that could protect the enzyme from oxidative damage.

Introduction

Hydrogenases are metalloenzymes that catalyze the reversible cleavage of molecular hydrogen into two protons and two electrons. According to the metal content of their active site, they are grouped into three phylogenetically unrelated classes: [Fe], [FeFe], and [NiFe] hydrogenases. Hydrogenases of the [Fe] and [FeFe] classes are synthesized exclusively under strictly anoxic conditions, whereas several [NiFe] hydrogenases are synthesized under oxic conditions and are catalytically active even in the presence of ambient O_2.[1]

The active site of [NiFe] hydrogenases consists of a nickel and an iron ion coordinated by four invariant cysteine residues. Two of them serve as terminal ligands to the nickel ion, and two are bridging ligands coordinating both the nickel and the iron ion. This configuration leaves a third bridging site, which can be vacant or occupied with hydrogen- or oxygen-based ligands under catalytic or inhibitory conditions, respectively.[2] The iron ion is additionally equipped with one carbon monoxide (CO) and two cyanide (CN^-) ligands, which give rise to one CO and two CN stretch vibrations. Changes in the structural and electronic properties of the active site and its immediate environment affect the frequencies of these vibrations, which can be monitored by infrared (IR) spectroscopy.[3–5] Thus, this technique is a powerful tool to investigate [NiFe] hydrogenases, and each redox-structural state of the active-site is most easily identified by its characteristic CO stretch frequency (see Table

S1 for CO and CN stretch frequencies assigned to the redox states discussed in this study). Electron paramagnetic resonance (EPR) spectroscopy provides complementary information on the electronic structure of paramagnetic redox states of the [NiFe] site.[6,7] Since the iron maintains a low-spin Fe^{II} configuration[1,8-11] in all known active-site states, EPR spectroscopy specifically probes the Ni ion, for which Ni^{III}, Ni^{II} and Ni^{I} states have been observed in [NiFe] hydrogenases.

[NiFe] hydrogenases can be further divided into four different groups depending on their structure, function, cellular location, and conserved sequence motifs.[12,13] Group 3 comprises a varied class of hetero-multimeric cytoplasmic [NiFe] hydrogenases, which possess additional subunits that are able to bind redox cofactors, such as F_{420}, NAD, or NADP. The NAD^+-reducing Soluble Hydrogenase from *Hydrogenophilus thermoluteolus* TH-1^T (*Ht*SH) is a prominent member of this group that couples the reversible cleavage of H_2 to the redox conversion of NAD. Due to its O_2 tolerance and thermostability, *Ht*SH is an attractive candidate for biotechnological applications, e.g. the regeneration of nucleotide cofactors.[14-16]

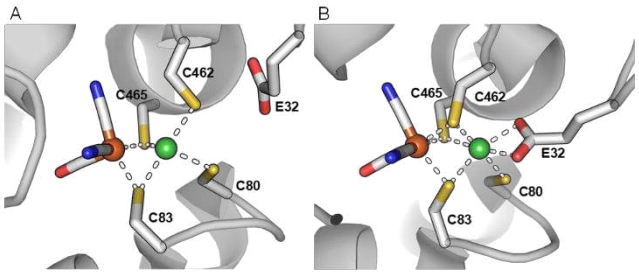

Figure 1. [NiFe] active-site structure of *Ht*SH. (A) H_2-reduced state (PDB: 5XFA), (B) oxidized state (PDB: 5XF9). The coordinating cysteine residues, the glutamate 32 residue, and the iron-coordinating CO and CN^- ligands are displayed as sticks. Iron and nickel are depicted by orange and green spheres, respectively. Dotted lines represent the ligand bonding between the metals and the amino acid residues. The figure has been generated using The PyMOL Molecular Graphics System, Version 2.2.0 Schrödinger, LLC.

Crystal structures of homologously produced *Ht*SH are available for the air-oxidized and H_2-reduced enzyme.[17] The oxidized [NiFe] site exhibits an unprecedented coordination geometry with a six-coordinate nickel site. Here, three bridging cysteines, one terminal cysteine, and the bidentate carboxylate group of glutamate residue E32 are bound to the nickel ion in a distorted octahedral fashion. In contrast, the reduced active site shows the typical configuration of [NiFe] hydrogenases (Figure 1).[17]

Similarly, IR spectra of reduced *Ht*SH exhibit absorption bands that can be assigned to typical catalytic intermediates, while the spectrum of the oxidized enzyme is remarkably different from those of all other [NiFe] hydrogenases.[16] This IR spectrum features an unprecedented high-frequency absorption band at 1993 cm^{-1}, which has been tentatively assigned to the CO stretch vibration of an oxidized [NiFe] state. Such a feature has not been reported for canonical (group-1) [NiFe] hydrogenases, indicating an unusual configuration of the active site.[16] These observations seem to suggest a relation between spectroscopic and crystallographic data, and the unusual configuration of the oxidized enzyme may represent a means to protect the [NiFe] site from O_2. However, an exact assignment and structural interpretation for the unusual IR feature is not available yet, and the configuration observed in the crystal phase may not reflect the native state of the enzyme that is observed in aqueous solution.[18] Moreover, structural insights into the interaction of *Ht*SH with O_2 are so-far missing.

Here, we use various biochemical and spectroscopic techniques to analyze Strep-tagged *Ht*SH (hereinafter referred to as 'native') and different amino acid exchange variants, all produced heterologously in *Ralstonia eutropha* and purified under aerobic conditions. Our data indicate that native *Ht*SH contains a modified [NiFe] site with a terminal glutamate ligand that can stabilize a tetravalent nickel ion. We demonstrate that this architecture is not a crystallization artefact but a specific response towards O_2, which is also observed in aqueous solution. Based on these findings, the O_2 protection mechanism of *Ht*SH will be discussed.

Results and Discussion

Due to limited sample concentrations, all IR absorption spectra in this study are presented as second derivatives, where absorption bands appear as sharp negative peaks. The unusual IR signal observed at 1993 cm^{-1} may correspond to a CO ligand bound to the [NiFe] active site of *Ht*SH, but the frequency is very high and unambiguous proof is still missing. To verify its assignment, we chose two approaches. (1) An *Ht*SH-producing *R. eutropha* derivative[16] was grown in the presence of $^{13}C^{18}O$ gas. This strategy was previously shown to yield mature hydrogenase featuring a [NiFe] active site with a labelled $^{13}C^{18}O$ ligand.[19,20] As expected for a quasi-diatomic oscillator, $^{13}C^{18}O$ labelling resulted in an isotopic shift of 87–91 cm^{-1} for all IR absorption bands between 1900 and 2000 cm^{-1}, including the unusual feature at 1993 cm^{-1} (Figure 2). This finding confirms that this absorption band reflects the stretching vibration of a hydrogenase-bound CO ligand. However, it does not reveal whether this CO ligand is bound to the active-site iron or another site of *Ht*SH. (2) To address this question, we used two-dimensional (2D) IR spectroscopy.[21] This technique allows determining the location of IR chromophores (e.g. CO) based on coupling and energy exchange with nearby molecular groups. Thus, if the CO ligand of interest is bound to the [NiFe] site (in an unusual fashion leading to a high CO stretch frequency), it should exhibit interactions with the tentatively assigned CN stretch modes at 2081 and 2090 cm^{-1}.[16,21] Indeed, cross signals between CO and CN stretch vibrations were observed, as best illustrated by pump slices through the 2D-IR spectrum (Figure 3A and B). Using frequency-domain terminology, these cross signals can be explained as follows. If *Ht*SH is pumped close to the absorption maximum of the CO stretch vibration (1994 cm^{-1}), negative signals corresponding to bleaching (and stimulated emission) of the CN stretch vibrations can be detected at probe frequencies of 2082 and 2091 cm^{-1} (Figure 3B). Likewise, pumping at CN stretch frequencies (2083 and 2091 cm^{-1}) yields a negative feature at 1996 cm^{-1}, indicating a depopulation of the CO stretch ground state (Figure 3A).

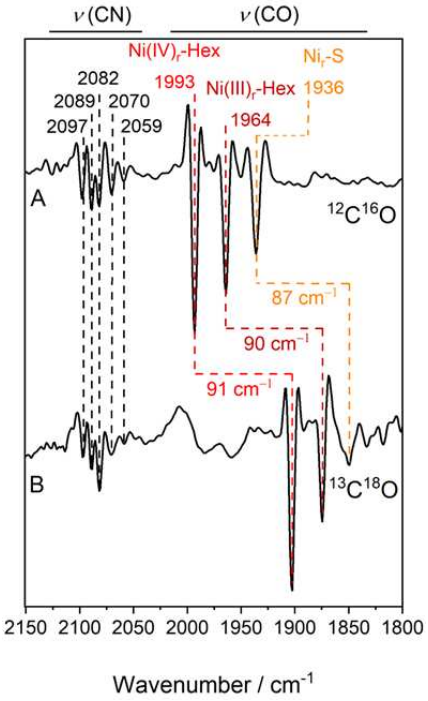

Figure 2. Second-derivative IR spectra of oxidized *Ht*SH isotopologues, measured at 283 K. (A) Native *Ht*SH containing naturally abundant $^{12}C^{16}O$. (B) *Ht*SH selectively labelled with $^{13}C^{18}O$. Spectral regions reflecting CO and CN stretch vibrations are indicated, and prominent signals are labelled. Assigned redox-structural states are discussed in the main text.

These observations confirm that the corresponding CO and CN stretch vibrations can be assigned to a single oxidized state of the enzyme, and their interaction indicates that both sets of ligands are bound to the active-site iron. Based on these results, we conclude that the absorption band at 1993 cm^{-1} reflects an iron-bound CO ligand, whose stretching frequency is exceptionally high due to peculiarities in the (electronic) structure of the heterobimetallic active site in oxidized *Ht*SH.

Next, we aimed to understand the molecular basis for the unusually high stretching vibration of the identified active-site CO ligand. According to crystal structure data,[17] this feature could reflect an active-site architecture with a bidentate glutamate ligand (E32) and three bridging cysteines, one of which serves as a terminal ligand in reduced *Ht*SH and all other [NiFe] hydrogenases (C462 in *Ht*SH). Since all active-site cysteines are essential to establish a functional [NiFe] center, C462 cannot be exchanged for other amino acids to directly explore its influence on IR spectroscopic properties of oxidized *Ht*SH. We therefore focused on E32, whose binding to a terminal Ni site – normally occupied by C462 – is anticipated to be key to the unusual geometry shown in Figure 1B.

We constructed three different *Ht*SH variants, in which E32 is replaced by glutamine (Q), alanine (A), or aspartate (D). These variants were purified by affinity chromatography (Figure S1), and their specific activity was measured as the H_2-driven reduction of NAD^+ to NADH at pH 6.5 and 50 °C (Figure 4). All three variants, E32Q, E32A, and E32D, showed very low activities corresponding to 0.2, 2.8, and 6.6 %, respectively, of that of native *Ht*SH. This drop in activity is comparable to observations for other [NiFe] hydrogenases[22-24] and can be explained by the lack of conserved E32 (*Ht*SH nomenclature), whose carboxylate side chain is involved in proton transfer during catalysis.[22-27] The E32A variant is ten-times more active than the E32Q variant, presumably due to the smaller size of the alanine side chain, which increases the chance to incorporate a water molecule or hydroxide ion that could facilitate proton transfer. The E32D variant shows the highest activity among the three variants (Figure 4), which becomes even clearer if the activity is normalized to the [NiFe] cofactor content per protein amount (Figure 4, Table S2). This finding agrees with observations for hydrogenases from *D. fructosovorans* and *E. coli*,[22,24] and it can be explained by the fact that aspartate may also act as proton acceptor, albeit less efficiently than glutamate due to its shorter carboxylate side chain.

To explore how glutamate E32 affects the active-site configuration, we first recorded IR spectra of all *Ht*SH variants in their as-isolated state (Figure 5, left; Figure S2). The previously reported IR spectrum of native *Ht*SH displays three CO stretch bands (Figure 5A), each reflecting a distinct redox-structural state. CO bands at 1964 and 1936 cm^{-1} have been previously assigned to the catalytically inactive and EPR-silent 'Ni_r-B-like' and Ni_r-S states, respectively.[16] As this assignment is partly challenged by our new results, we will refer to both states by their CO stretch frequency in the subsequent paragraphs. As demonstrated by isotope labeling and 2D-IR spectroscopy (vide supra), the third absorption band at 1993 cm^{-1} also reflects an active-site CO stretch mode, which – based on its high frequency – is assigned to a state at or above the Ni_r-B redox level.[16]

The IR spectrum of the E32D variant (Figure 5B) is similar to that of native *Ht*SH. However, the positions of all three CO stretch bands are systematically shifted by 5–7 cm^{-1} towards higher frequencies, resulting in absorption maxima at 1998, 1969, and 1943 cm^{-1}. The CN stretch frequencies seem to be shifted to a similar extent, but not all corresponding absorption bands could be identified, due to the lower overall intensity of the IR spectrum of the E32D variant. We suspect that these shifts reflect a redistribution of electronic charge at the active site, caused by a change in the dielectric properties of the environment that may be linked, *inter alia*, to a displacement and/or reorientation of the carboxylate function of the shorter aspartate side chain. Notably, these shifts are more pronounced than those observed for the corresponding variant of the [NiFe] hydrogenase from *D. fructosovorans*,[22] indicating a more flexible active-site environment in *Ht*SH. This finding is in line with the large-scale structural rearrangements necessary for interconverting oxidized and reduced *Ht*SH.[17]

IR spectra of the E32A and E32Q variants of *Ht*SH exhibit dominant CO stretch bands at 1971/1943 and 1974/1941 cm^{-1}, respectively (Figures 5C and 5D), analogous to signals at 1964/1936 cm^{-1} observed for native *Ht*SH. Further weaker CO stretch bands, reflecting oxidized side species, are detected at, e.g., 1960 and 1949 cm^{-1} for both *Ht*SH variants. In line with the multitude of CO stretch signals, several partly broadened CN stretch bands can be observed as well (Figure S2). These features differ clearly from those observed for the native *Ht*SH and the E32D species, but the overall band patterns detected for E32A and E32Q variants

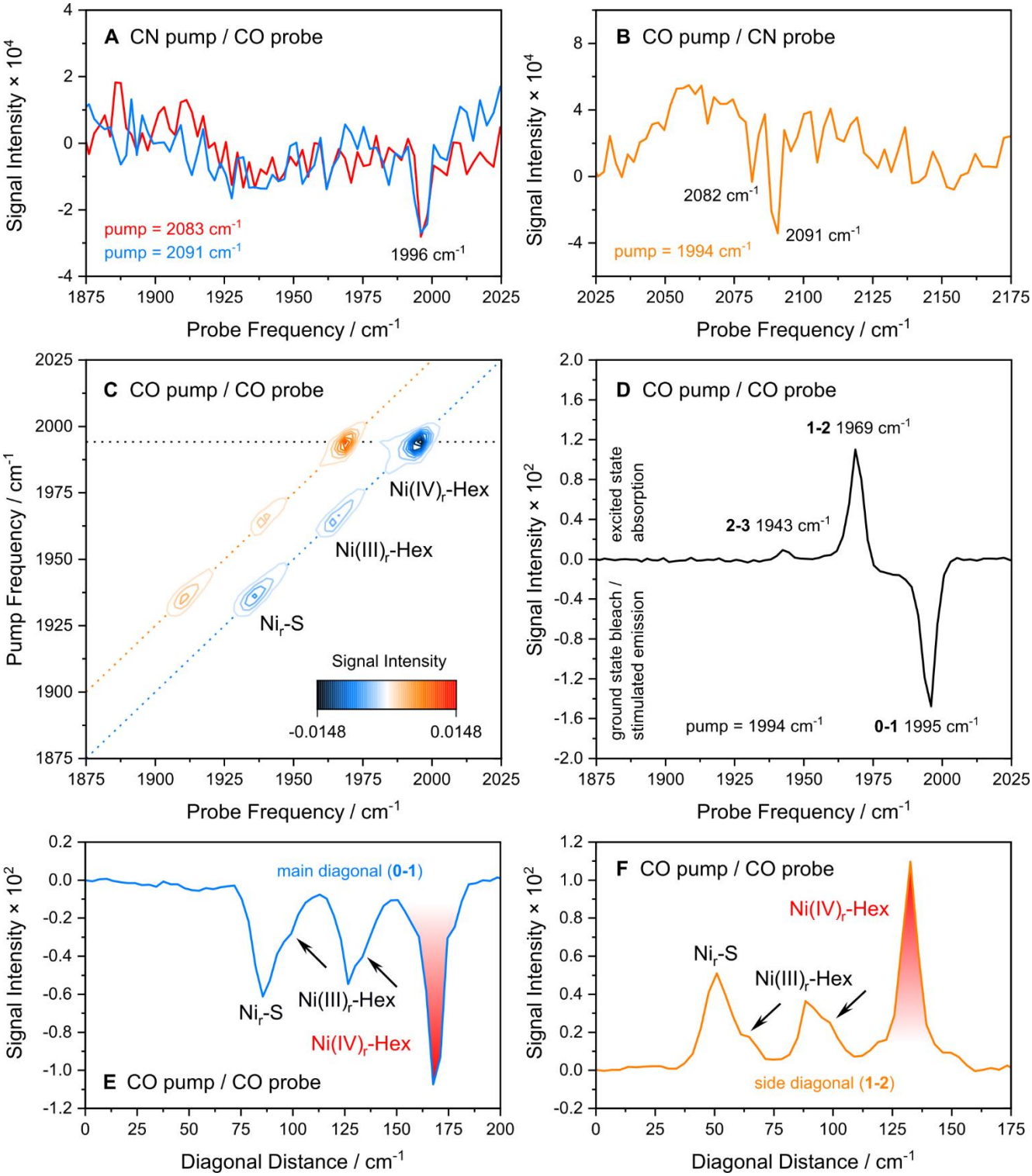

Figure 3. 2D-IR spectra of oxidized *Ht*SH, recorded with perpendicular pump-probe polarization. (A) Pump slice through the 2D-IR spectrum reflecting CO stretch bleaching (and stimulated emission) upon excitation of Ni(IV)$_r$-Hex CN stretch modes. (B) Pump slice through the 2D-IR spectrum reflecting CN stretch bleaching (and stimulated emission) upon Ni(IV)$_r$-Hex CO stretch excitation. (C) 2D-IR contour plot of the diagonal CO stretch region. Locations of a Ni(IV)$_r$-Hex pump slice (see D) and two diagonal slices (see E and F) are indicated as color-coded dotted lines. (D) Pump slice reflecting Ni(IV)$_r$-Hex CO stretch transitions (up to the third vibrational level; see C). (E) Main diagonal through the CO stretch region of the 2D-IR spectrum (see C), reflecting ground state bleaching and stimulated emission associated with 0-1 (ground-state absorption) transitions. (F) Side diagonal through the CO stretch region of the 2D-IR spectrum (see C), reflecting transient absorption associated with the 1-2 (first-excited-state absorption) transitions. Arrows in plots E and F indicate minor subforms of Ni$_r$-S and Ni(III)$_r$-Hex states. Spectra in A and B were recorded at a waiting time of T_w = 15 ps. All other data were acquired at T_w = 250 fs. Samples for 2D-IR measurements were additionally purified by size-exclusion chromatography.

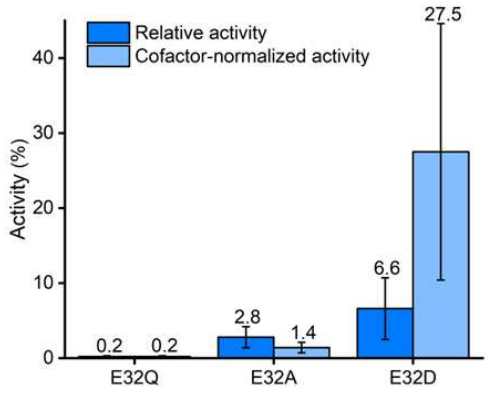

Figure 4. H_2-oxidation activity of E32X variants in relation to native *Ht*SH activity. The reduction of NAD^+ to NADH was measured at 50 °C in H_2-saturated buffer. 100 % corresponds to a specific activity of (22.1 ± 4.2) U mg^{-1}. Relative activity of *Ht*SH variants E32Q, E32A and E32D (dark blue). Relative activities of E32Q, E32A and E32D variants (light blue) normalized to the [NiFe] cofactor content per protein. Absolute, relative, and normalized activities are listed in Table S2.

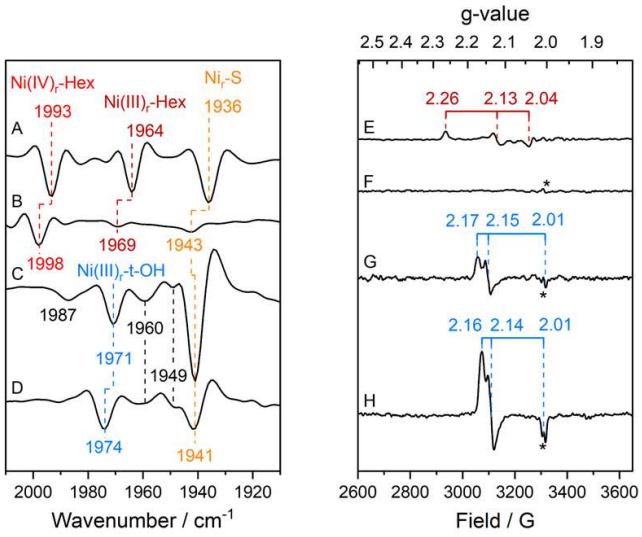

Figure 5. Second-derivative IR spectra (left) and EPR spectra (right) of native *Ht*SH and its E32 exchange variants in their as-isolated, oxidized form. (A, E) Native *Ht*SH, (B, F) E32D, (C, G) E32A, and (D, H) E32Q variants. IR and EPR spectra were recorded at 283 and 80 K, respectively. IR spectra only depict the spectral regime associated with the CO stretch vibration; the CN stretch region is included in Figure S2. EPR signals labeled with an asterisk (g = 2.01) most likely correspond to negligible contributions from flavin mononucleotide radicals.

are similar to each other. Most importantly, the dominating high-frequency CO stretch band – observed at 1993 cm^{-1} for native *Ht*SH and 1998 cm^{-1} for the E32D species – is absent in the IR spectra of the E32A and E32Q variants (Figure 5). These observations demonstrate that the CO stretch band at 1993 (1998) cm^{-1} represents a redox-structural state that depends on interactions between the carboxylate side chain of E32 (D32) and the active site. This supports the idea that this state features terminal glutamate coordination, as reflected by the crystal structure of oxidized native *HtSH* (Figure 1B). To test the hypothesis that this unusual coordination pattern is also responsible for the high CO stretch frequency, we used density functional theory (DFT) for calculating IR spectra of different redox-structural states (see Table S3 for a complete overview).[28–31] Surprisingly, we found that the unusual coordination pattern gives rise to a CO stretch frequency that is almost indistinguishable from that observed for a redox-equivalent state with a bridging OH^- ligand, two terminal cysteines, and two bridging cysteines (as proposed for Ni_r-B and Ni_r-S states; Figure 6A).

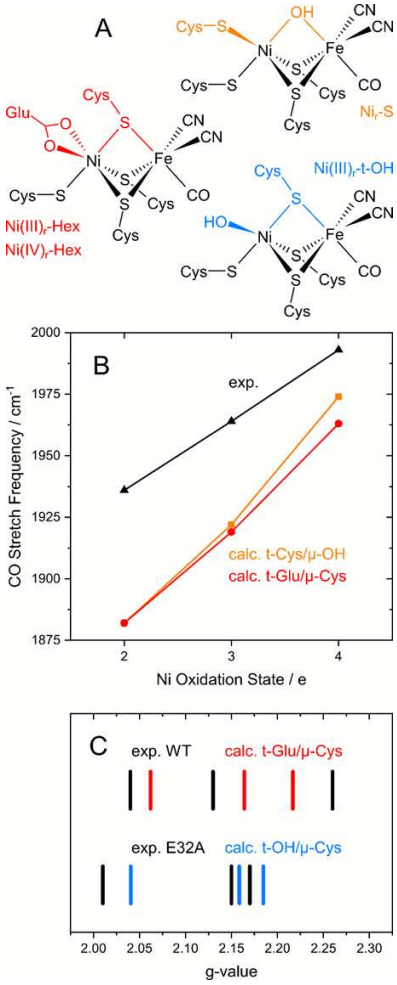

Figure 6. Comparison between experimental and calculated IR and EPR spectroscopic properties. (A) Structural models considered for different active-site states of *Ht*SH. Variable terminal (t) and bridging (μ) ligands are color-coded. Experimentally detected redox-structural states sharing these coordination motifs are indicated. (B) CO stretch frequency as a function of the formal Ni oxidation state. Plotted frequency trends correspond to experimental data (black) and two computational models reflecting the depicted coordination patterns (orange and red). (C) Comparison of experimental g-values of wildtype *Ht*SH and the E32A variant with those calculated for the depicted coordination patterns (red and light blue). For details and further computational results, see main text, Figure S4, Table S3, Table S4, and atomic coordinates reported in the Supporting Information.

This indicates that the high-frequency CO stretch band cannot be explained by glutamate coordination alone. However, the experimental frequency trend observed for oxidized *Ht*SH – three absorption bands separated by ca. 30

cm^{-1} – is well reproduced by a computational scenario in which the three signals reflect different Ni oxidation states, i.e. Ni(II), Ni(III), and Ni(IV) (Figure 6B; Figure S4). Thus, we propose that the high CO stretch frequency observed for fully oxidized *Ht*SH reflects an active-site species with a formal Ni(IV) ground state that is stabilized by a six-coordinate ligand sphere involving E32, as observed in the crystal structure of the oxidized enzyme. As this unprecedented redox-structural state is readily activated by H_2 (Figure S5),[16,17] we assign it to a 'ready' stated called $Ni(IV)_r$-Hex.

Since the coordination pattern reflected by the crystal structure cannot be clearly distinguished from other structural scenarios by IR spectroscopy alone (Figure 6, Figure S4, Table S3, and Table S4), we also recorded EPR spectra at 80 K (Figure 5, right; Table S5) to gain further insight into the different *Ht*SH variants and their redox-structural states. In line with a previous report,[16] the EPR spectrum of the as-isolated native enzyme (Figure 5E) exhibits no signals corresponding to IR features at 1936 and 1993 cm^{-1}, supporting our assignment to Ni(II) and Ni(IV) oxidation states, respectively. In contrast to other oxidized group-3 hydrogenases,[32–38] however, we observe a previously reported rhombic signal (g_x = 2.26, g_y = 2.13, g_z = 2.04),[17] indicative of a Ni(III) species, which was barely populated in our first study.[16] This state is easily activated by H_2 (Figure S5), and its population correlates with the IR signal at 1964 cm^{-1}. Thus, we assign both features to a 'ready' state at the Ni_r-B redox level (Figure 5A) whose EPR signature differs markedly from that of a typical Ni_r-B state,[39] though. The population of this state is very low for the E32D variant (Figure 5B), so that the corresponding EPR spectrum does not exhibit any distinct paramagnetic species (Figure 5F). In contrast, E32A and E32Q variants exhibit another unique rhombic signature (Figure 5G and 5H) that is clearly distinguishable from the one observed for native *Ht*SH. According to relative signal intensities of EPR and IR spectra, this signature is likely associated with a Ni(III) state characterized by CO bands at 1971 (E32A) and 1974 cm^{-1} (E32Q). In contrast to expectations, the absence of E32 in these variants does not give rise to a typical Ni_r-B signal. Instead, the observed EPR signature differs markedly from the rhombic signal reported for this [NiFe] intermediate[39] and also from that observed for the native enzyme. We propose that these spectroscopic peculiarities originate from an inversion of the Cys–Ni–OH configuration observed for Ni_r-B (Figure 6A, orange), in which C462 is still bound to the third bridging site between Ni and Fe, while E32, which is absent in these variants, is replaced by a terminal OH^- ligand (Figure 6A, blue). This hypothesis is supported by DFT calculations that qualitatively reproduce the almost axial g-tensor observed in the EPR spectra of E32A and E32Q variants (Figure 6C). Based on the proposed structure, we tentatively refer to this state as $Ni(III)_r$-t-OH.

The above findings demonstrate that Ni(III) states observed for native *Ht*SH and E32A/E32Q variants are not structural analogues. Given the sensitivity of the EPR signature to the glutamate exchange, we propose that the Ni(III) state of native *Ht*SH, characterized by the CO stretch band at 1964 cm^{-1}, also features six-fold coordination involving a terminal glutamate (in contrast to the E32A/E32Q variants). Thus, we call this state $Ni(III)_r$-Hex. This proposal is in line with our DFT calculations (Figure 6; Figure S4) and further supported by IR spectra recorded from crystals of oxidized native *Ht*SH (Figure S6). These spectra show that crystallized *Ht*SH features a mixture of states similar to those observed in solution, but X-ray diffraction did not reveal structural contributions other than the six-coordinate configuration (Figure 1B). This suggests that all notable species of the mixture share this structural motif, including the dominating $Ni(III)_r$-Hex state and its subforms (*vide infra*).

Neither IR nor EPR spectroscopy provides direct information on the structure of the native Ni(II) state, characterized by the CO stretch band at 1936 cm^{-1} (Fig. 5A). As this Ni(II) state is barely populated in oxidized *Ht*SH crystals (Figure S6), its structural features may not be reflected by the published X-ray diffraction data. DFT calculations, however, indicate that a six-fold coordination is less likely for Ni(II) (Table S3). In that case, glutamate clearly favors monodentate coordination, and one of the bridging cysteines dissociates from nickel. This structural reorganization yields a square-planar Ni coordination geometry, as expected for a four-coordinate low-spin d^8 transition metal center. Imposing additional structural constraints (see Tables S5 and S6) did not lead to a stable six-coordinate geometry either. Thus, we propose that the Ni(II) state of as-isolated *Ht*SH features a conventional coordination geometry with a bridging OH^- ligand, two bridging cysteines and two terminal cysteines (as proposed for the previously assigned Ni_r-S state) in both the native enzyme and its E32X variants.

In total, our spectroscopic and theoretical results suggest that as-isolated *Ht*SH features an unusual active-site configuration with a terminal carboxylate side chain coordinating the Ni ion in its tri- and tetravalent forms. This glutamate coordination, which is most likely accompanied by a transfer of the terminal C462 residue to the third bridging position of the [NiFe] site, reflects a six-coordinate Ni ion and agrees well with available crystal-structure data (Figure 1B).[17] Our data provide the first evidence that this configuration represents a biologically relevant feature of the enzyme that is also formed in aqueous solution under physiologically relevant conditions.

To gain further structural insights into the active-site states of as-isolated native *Ht*SH, we returned to 2D-IR spectroscopy. Accessing transitions involving multiple vibrationally excited states (Figures 3C and D), nonlinear IR spectroscopy allows determining fundamental bond properties by fitting a Morse potential to experimental transition energies of a (quasi-)diatomic oscillator.[21] This analysis reveals that the equilibrium bond strength (expressed by the force constant) of the active-site CO ligand increases with the Ni oxidation state (Ni_r-S < $Ni(III)_r$-Hex < $Ni(IV)_r$-Hex; Table 1). Consistently, $Ni(IV)_r$-Hex appears to feature a weaker Fe–CO bond than Ni_r-S, as concluded from the longer CO-stretch vibrational lifetime, i.e. less efficient energy transfer towards the [NiFe] core (Figure 7; see Material & Methods for a detailed discussion). Force constants from the Morse analysis and empirical relations also reveal solution-phase bond lengths.[40] Using this approach and an adequate expression for CO oscillators,[41] we derive solution-phase CO bond lengths of 1.153, 1.148, and 1.141 Å for Ni_r-S, $Ni(III)_r$-Hex, and $Ni(IV)_r$-Hex, respectively (Table 1). The latter two values agree well with the exceptionally short bond length of

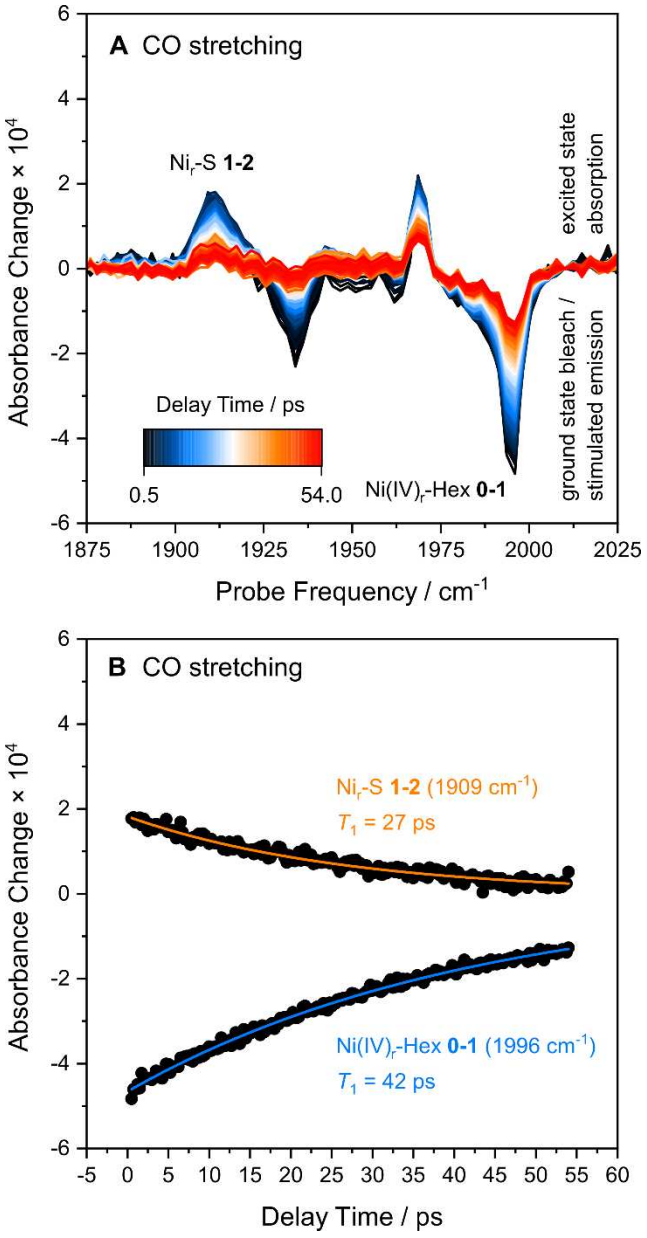

Figure 7. Vibrational dynamics of oxidized *Ht*SH. (A) Broadband IR_{pump}-IR_{probe} spectra, recorded with parallel polarization. (B) Time evolution of first excited states of Ni_r-S and $Ni(IV)_r$-Hex, derived from transitions highlighted in A. Indicated population lifetimes T_1 were obtained by fitting monoexponential decay curves to the experimental data. Due to strong overlap and cancellation of signals, no reliable vibrational lifetime could be obtained for the $Ni(III)_r$-Hex state. Samples for IR_{pump}-IR_{probe} measurements were additionally purified by size-exclusion chromatography.

1.142 Å reflected by the crystal structure,[17] supporting our assignment. While bond lengths and equilibrium bond strengths exhibit clear trends, total CO bond strengths (dissociation energies) of all three active-site states of as-isolated *Ht*SH are almost identical (Table 1). While the details and implications of this observation are beyond the scope of this paper, our finding indicates that the oft-quoted simple relation between 'bond strength' and vibrational frequency may fall short. Finally, analysis of 2D-IR diagonals (Figure 3E and F) reveals two or more distinguishable subforms of Ni_r-S and $Ni(III)_r$-Hex but not $Ni(IV)_r$ Hex. This indicates that $Ni(IV)_r$-Hex is structurally more constrained (less flexible and thus preventing the formation of isomeric subforms), which agrees with its six-fold coordination pattern and the fact that E32 appears to be more tightly bound in $Ni(IV)_r$-Hex than in $Ni(III)_r$-Hex (see Table S3). We also note that the $Ni(IV)_r$-Hex state exhibits a peculiar (2D) lineshape (Figure 3C,E and F), implying a unique distribution of underlying microstates that demands further investigation in the future.

Table 1. CO bond properties of oxidized *Ht*SH.*

Redox State	$\nu_{0\text{-}1}$ (cm^{-1})	ν_0 (cm^{-1})	f (Nm^{-1})	$2\nu_0\chi$ (cm^{-1})	D_0 (kJ mol^{-1})	d (Å)
Ni_r-S	1935.7	1960.1	1553.0	24.5	926.3	1.153
$Ni(III)_r$-Hex	1964.1	1989.2	1599.4	25.3	925.4	1.148
$Ni(IV)_r$-Hex	1995.0	2020.9	1650.8	26.0	929.3	1.141

* $\nu_{0\text{-}1}$, fundamental frequency; ν_0, harmonic frequency; f, force constant (equilibrium bond strength); $2\nu_0\chi$, anharmonic shift (average separation between neighboring spectroscopic lines); D_0, zero-point dissociation energy (total bond strength); d, bond length.

Insights into the functional roles of the two Ni_r-Hex states can be derived from the O_2 dependence of their formation. As reported previously, as-isolated *Ht*SH (Figure 8A and 8D) readily forms catalytically relevant Ni_a-C and Ni_a-SR states upon reduction.[16] Subsequent exposure to air leads to reoxidation of the enzyme and the predominant formation of the EPR-silent $Ni(IV)_r$-Hex state (Figures 8B and 8E). Interestingly, formation of $Ni(IV)_r$-Hex is not observed upon anaerobic reoxidation with ferricyanide (Figure 8C and 8F). Under these conditions, $Ni(III)_r$-Hex is enriched instead, in line with previous observations from spectroelectrochemical studies.[16] Notably, the formed $Ni(III)_r$-Hex population can be rapidly re-activated by H_2 treatment, and subsequent incubation of the reduced *Ht*SH with O_2 results in the formation of $Ni(IV)_r$-Hex (Figure S7). These findings demonstrate that the high-valent $Ni(IV)_r$-Hex state is not a purification artefact but a specific and reversible structural response towards O_2. Consistent with this statement, the relative amount of $Ni(IV)_r$-Hex critically depends on the reoxidation procedure. If reduced *Ht*SH is reoxidized by slow diffusion of air into the IR cell, Ni_r-S and $Ni(III)_r$-Hex states are formed in addition to $Ni(IV)_r$-Hex (Figure S8B), resulting in a spectrum reflecting an equilibrium mixture similar to that observed for as-isolated *Ht*SH (Figure S8A). In contrast, fast exposure to air yields a strong enrichment of the $Ni(IV)_r$-Hex state (Figure S8C). This indicates that formation of this state is kinetically favored under strongly oxic conditions, which suggests that this structural and electronic configuration serves as a specific response to O_2 that could protect the active site from irreversible damage. Further support for this hypothesis comes from the fact that $Ni(IV)_r$-Hex is formed before $Ni(III)_r$-Hex during slow oxidation by O_2 (Figure S9). This observation indicates that $Ni(IV)_r$-Hex is a kinetic rather than a thermodynamic product and, thus, unlikely to reflect a mere response to high potential.

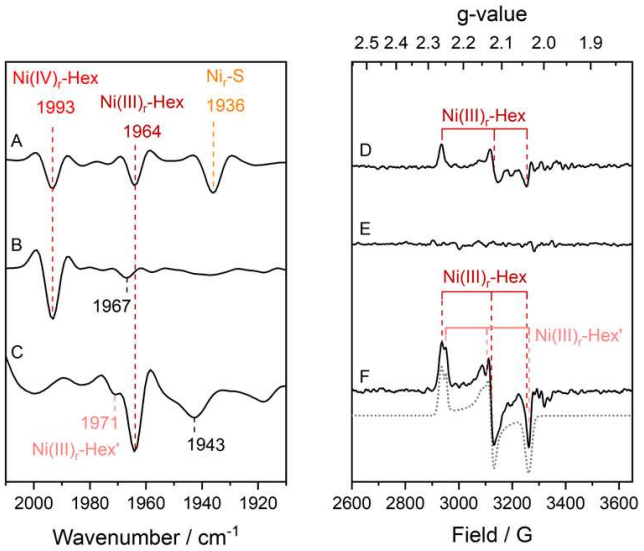

Figure 8. Second-derivative IR spectra (left) and EPR spectra (right) of as-isolated native *Ht*SH (A, D), *Ht*SH after H_2 reduction and subsequent aerobic reoxidation with air (B, E), and *Ht*SH after H_2 reduction and subsequent anaerobic reoxidation with $K_3Fe(CN)_6$ (C, F). IR spectra only depict the spectral regime associated with the CO stretch vibration; the CN stretch region and further details are presented in Figures S10 and S11. IR and EPR spectra were recorded at 283 K and 80 K, respectively. The simulation sum of the $Ni(III)_r$-Hex subspecies is indicated by a grey dotted line. The individual simulated spectra are displayed in Figure S11, and corresponding g-values are listed in Table S5.

Conclusion

Using selective $^{13}C^{18}O$ labelling and (2D-)IR spectroscopy, we have demonstrated that the high-frequency infrared signal observed for oxidized *Ht*SH can be assigned to the stretching vibration of an active-site-bound CO ligand. IR and EPR analyses of amino acid exchange variants revealed that this signal corresponds to one of at least two [NiFe] states, designated as Ni_r-Hex, that feature a six-coordinate Ni with a terminal glutamate (E32) ligand, as observed in the crystal structure of oxidized *Ht*SH.[17] This finding is further supported by a good match between the crystal structure and the 2D-IR-derived solution-phase CO bond lengths of these states. In line with crystal-phase IR spectra, we therefore conclude that the crystal structure of oxidized *Ht*SH reflects a mixture of native active-site states that are also formed in aqueous solution.

While spectroscopic studies on amino acid exchange variants reveal glutamate coordination for both Ni_r-Hex states, quantum chemical calculations demonstrate that the high CO stretch frequency observed for one of them cannot be explained by glutamate coordination and the formation of a six-coordinate Ni center alone. Instead, our calculations indicate that this high frequency reflects a biologically unprecedented Ni(IV) ground state, in line with the EPR data and a previously proposed involvement of tetravalent Ni in hydrogenase function.[42] Besides its unusual coordination geometry and high formal oxidation state, this unique configuration, called $Ni(IV)_r$-Hex, exhibits a strained active-site geometry, a soft Fe–CO metal-ligand bond, and an unusually stiff and short but not overly strong CO bond, as revealed by 2D-IR and IR_{pump}-IR_{probe} data.

In addition to insights into the structure and dynamics of the $Ni(IV)_r$-Hex state, our data also reveal its functional significance. While $Ni(III)_r$-Hex can be enriched in the absence of O_2 at mildly oxidizing potentials, the $Ni(IV)_r$-Hex state is rapidly, specifically, and reversibly formed under oxic conditions, especially upon sudden exposure of catalytic intermediates to high O_2 concentrations. This indicates that the formation of $Ni(IV)_r$-Hex represents a kinetically controlled protective response towards O_2. In this respect, bidentate nickel coordination by E32 and the additional movement of cysteine C462 from a terminal site to a bridging position between Ni and Fe may prevent oxidative damage in two ways. On the one hand, the coordinatively saturated [NiFe] site is sterically shielded from O_2 attack. On the other hand, both E32 and C462 are unable to take over their normal function as proton relays, thereby preventing proton transport to the active site, which in turn limits the formation of reactive oxygen species (ROS). $Ni(III)_r$-Hex could also be involved in these processes, but the lower Ni oxidation state leads to a weaker binding of E32, which likely impedes its protective function. Thus, we propose that $Ni(IV)_r$-Hex represents the key element in the O_2 protection mechanism of *Ht*SH.

Notably, formation and reactivation of $Ni(IV)_r$-Hex involves considerable structural rearrangement,[17] which can explain why *Ht*SH is catalytically less active under oxic conditions than some other O_2-tolerant (group-3) hydrogenases.[16,] For instance, the similar NAD^+-reducing hydrogenase from the mesophile *R. eutropha* retains full activity at 20 % O_2 by catalytically detoxifying O_2.[28,43] In contrast, $Ni(IV)_r$-Hex represents a resting state whose primary function is not to sustain H_2 cycling under high O_2 levels but rather to protect *Ht*SH and maybe other cellular constituents from irreversible damage related to metal-assisted ROS production. By increasing molecular connectivity in the active site region, sixfold coordination observed for this state may also add to the temperature stability of the enzyme in cases where oxidative stress and elevated temperatures are correlated.

So far, it is unclear how the formation of $Ni(IV)_r$-Hex is specifically triggered by O_2. Since this state does not contain O_2-derived ligands or modifications,[17] initiation of the protective process likely occurs before O_2 reaches the [NiFe] center. This may involve other reactive sites of the enzyme, consistent with associated changes of the protein matrix. Indeed, the crystal structure of oxidized *Ht*SH reveals large amino acid side chain displacements of residues located in proximity of the [NiFe] site and the nearby [4Fe-4S] cluster, Y1, which could indicate that formation of $Ni(IV)_r$-Hex depends on the redox state of this Y1 cluster.[17] However, the O_2 specificity of such a mechanism is unintelligible, and no indications for interactions of this [4Fe-4S] cluster with O_2 or ROS have been reported. Thus, we hypothesize that initial O_2 sensing may rather occur at the FMN cofactor, which is known to readily react with O_2, e.g., in other group-3 hydrogenases and homologous respiratory complex I (*vide supra*).[43] While the exact mechanism of the putative sensing and signal transduction events is unclear, it could involve intramolecular redox signaling *via* the enzyme's FeS clusters, possibly including the mentioned [4Fe-4S] center.

Finally, we like to highlight intriguing similarities between the proposed protective mechanism and other metalloenzymes. Recently, a conserved cysteine residue was found to shield the substrate binding site of an [FeFe] hydrogenase from O_2 attack, thereby preventing active-site from ROS-induced degradation.[44] While it is unclear how the formation of this inactive but protected state may be triggered by O_2, active-site shielding was found to involve structural reorganization remote from the active site and over-oxidation of the [FeFe] center. Another example, even more similar to *Ht*SH, can be found in superoxide reductase (SOR), a non-heme iron enzyme involved in the reductive detoxification of O_2^-.[45-47] The active site of some SORs features glutamate binding in the oxidized resting state,[48-51] thereby creating a coordinatively saturated active site that is unable to take part in undesired side reactions that could, e.g., convert the enzymatic H_2O_2 product into highly reactive •OH. Glutamate binding is reversible upon reductive activation,[48,49] involving a global rearrangement of the protein, which may be relevant for inter-site communication during (de-)activation.[48] In total, reversible binding of glutamate or other suitable ligands, triggered by an off-site redox stimulus, may represent a general mechanism for preventing undesired reactions of catalytic metal sites with O_2 or ROS.

ASSOCIATED CONTENT

Supporting Information.
This material is available free of charge *via* the Internet at http://pubs.acs.org."
Materials and Methods, supporting spectroscopic and DFT data

AUTHOR INFORMATION

Corresponding Author

Oliver Lenz – Institut für Chemie, Technische Universität Berlin, 10623 Berlin, Germany; orcid.org/ 0000-0003-4550-5128; Email: oliver.lenz@tu-berlin.de

Ingo Zebger – Institut für Chemie, Technische Universität Berlin, 10623 Berlin, Germany; orcid.org/0000-0002- 6354-3585; Email: ingo.zebger@tu-berlin.de

Marius Horch - Freie Universität Berlin, Fachbereich Physik, Arnimallee 14, D-14195 Berlin, Germany; orcid.org/0000-0001-6656-1749; Email: marius.horch@fu-berlin.de

Author Contributions

‡C. J. K-P., A.-C. S. and C. L. contributed equally.

Funding Sources

This work was supported by the Deutsche Forschungsgemeinschaft (DFG, German Research Foundation) as part of the SPP 1927 within the projects 10043725 (ZE 510/2-1), 10043724 (LE 2934/1-1), 311062227 (ZE 510/2-2) and 311062227 (LE 2934/1-2), and under Germany's Excellence Strategy—EXC 2008/1–390540038 ("Unifying Systems in Catalysis—UniSysCat"). O.L. and I.Z. are grateful for funding from the EU's Horizon 2020 research and innovation programme under grant agreement No 810856. S. L. D. W., B. P., N. T. H., and M.H. thank the Leverhulme Trust (RPG-2018-188) for financial support. C. C. M. B. and M.H. are grateful for financial support by the Einstein Foundation Berlin. Y.H. thanks the MEXT KAKENHI Grants-in-Aid for Scientific Research on Innovative Areas (Hydrogenomics) (No.18H05516) and JSPS KAKENHI Grants-in-Aid for Scientific Research (A) (No. 19H00984). The authors thank the STFC for funding access to the ULTRA laser system at the STFC Central Laser Facility (20130007).

Notes

The authors declare no competing financial interest.

ACKNOWLEDGMENT

The authors would like to acknowledge Giorgio Caserta (Technische Universität Berlin) for helping with sample preparation and handling, Matthias Stein (Max Planck Institute for Dynamics of Complex Technical Systems) for preliminary DFT calculations, and Kiriko Hataguchi and Kayoko Matsumoto (University of Hyogo) for their support with enzyme preparation.

REFERENCES

(1) Cammack, R.; Frey, M.; Robson, R. Hydrogen as a Fuel: Learning from Nature; Taylor & Francis Inc.: London and New York, **2001**.

(2) Volbeda, A.; Charon, M.-H.; Piras, C.; Hatchikian, E. C.; Frey, M.; Fontecilla-Camps, J. C. Crystal Structure of the Nickel-Iron Hydrogenase from *Desulfovibrio gigas*. *Nature* **1995**, *373*, 580–587.

(3) Pierik, A. J.; Roseboom, W.; Happe, R. P.; Bagley, K. A.; Albracht, S. P. J. Carbon Monoxide and Cyanide as Intrinsic Ligands to Iron in the Active Site of [NiFe]-Hydrogenases. $NiFe(CN)_2CO$, Biology's Way to Activate H_2. *J. Biol. Chem.* **1999**, *274* (6), 3331–3337.

(4) Happe, R. P.; Roseboom, W.; Pierik, A. J.; Albracht, S. P. J.; Bagley, K. A. Biological Activation of Hydrogen. *Nature* **1997**, *385* (6612), 126.

(5) Volbeda, A.; Garcin, E.; Piras, C.; De Lacey, A. L.; Fernandez, V. M.; Hatchikian, E. C.; Frey, M.; Fontecilla-Camps, J. C. Structure of the [NiFe] Hydrogenase Active Site: Evidence for Biologically Uncommon Fe Ligands. *J. Am. Chem. Soc.* **1996**, *118* (51), 12989–12996.

(6) Teixeira, M.; Moura, I.; Xavier, A. V.; Huynh, B. H.; DerVartanian, D. V.; Peck, H. D.; LeGall, J.; Moura, J. J. G. Electron Paramagnetic Resonance Studies on the Mechanism of Activation and the Catalytic Cycle of the Nickel-Containing Hydrogenase from *Desulfovibrio gigas*. *J. Biol. Chem.* **1985**, *260* (15), 8942–8950.

(7) LeGall, J.; Ljungdahl, P. O.; Moura, I.; Peck, H. D.; Xavier, A. V.; Moura, J. J. G.; Teixera, M.; Huynh, B. H.; DerVartanian, D. V. The Presence of Redox-Sensitive Nickel in the Periplasmic Hydrogenase from *Desulfovibrio gigas*. Biochem. *Biophys. Res. Commun.* **1982**, *106* (2), 610–616.

(8) Dole, F.; Fournel, A.; Magro, V.; Hatchikian, E. C.; Bertrand, P.; Guigliarelli, B. Nature and Electronic Structure of the Ni-X Dinuclear Center of *Desulfovibrio gigas* Hydrogenase. Implications for the Enzymatic Mechanism. *Biochemistry* **1997**, 36 (25), 7847–7854.

(9) Surerus, K. K.; Münck, E.; Chen, M.; van der Zwaan, J. W.; Kolk, M.; Duin, E. C.; Rusnak, F. M.; Albracht, S. P. J. Further Characterization of the Spin Coupling Observed in Oxidized Hydrogenase from *Chromatium vinosum*. A Mössbauer and Multifrequency EPR Study. *Biochemistry* **1994**, 33 (16), 4980–4993.

(10) Huyett, J. E.; Carepo, M.; Pamplona, A.; Franco, R.; Moura, I.; Moura, J. J. G.; Hoffman, B. M. ^{57}Fe Q-Band Pulsed ENDOR of the Hetero-Dinuclear Site of Nickel Hydrogenase: Comparison of the NiA, NiB, and NiC States. *J. Am. Chem. Soc.* **1997**, 119 (39), 9291–9292.

(11) Roncaroli, F.; Bill, E.; Friedrich, B.; Lenz, O.; Lubitz, W.; Pandelia, M.-E. Cofactor Composition and Function of a H_2-Sensing Regulatory Hydrogenase as Revealed by Mössbauer and EPR Spectroscopy. *Chem. Sci.* **2015**, 6 (8), 4495–4507.

(12) Vignais, P. M.; Billoud, B. Occurrence, Classification, and Biological Function of Hydrogenases: An Overview. *Chem. Rev.* **2007**, *107* (10), 4206–4272.

(13) Greening, C.; Biswas, A.; Carere, C. R.; Jackson, C. J.; Taylor, M. C.; Stott, M. B.; Cook, G. M.; Morales, S. E. Genomic and Metagenomic Surveys of Hydrogenase Distribution Indicate H_2 Is a Widely Utilised Energy Source for Microbial Growth and Survival. *ISME J.* **2015**, *10* (3), 761–777.

(14) Lauterbach, L.; Lenz, O.; Vincent, K. A. H_2-Driven Cofactor Regeneration with NAD(P)$^+$-Reducing Hydrogenases. *FEBS J.* **2013**, *280*, 3058–3068.

(15) Ratzka, J.; Lauterbach, L.; Lenz, O.; Ansorge-Schumacher, M. B. Systematic Evaluation of the Dihydrogen-Oxidising and NAD$^+$-Reducing Soluble [NiFe]-Hydrogenase from *Ralstonia eutropha* H16 as a Cofactor Regeneration Catalyst. *Biocatal. Biotransformation* **2011**, *29* (6), 246–252.

(16) Preissler, J.; Wahlefeld, S.; Lorent, C.; Teutloff, C.; Horch, M.; Lauterbach, L.; Cramer, S. P.; Zebger, I.; Lenz, O. Enzymatic and Spectroscopic Properties of a Thermostable [NiFe]-hydrogenase Performing H_2-Driven NAD$^+$-Reduction in the Presence of O_2. *Biochim. Biophys. Acta - Bioenerg.* **2018**, *1859* (1), 8–18.

(17) Shomura, Y.; Tai, H.; Nakagawa, H.; Ikeda, Y.; Ishii, M.; Igarashi, Y.; Nishihara, H.; Ogo, S.; Hirota, S.; Higuchi, Y. Structural Basis of the Redox Switches in the NAD$^+$-Reducing Soluble [NiFe]-Hydrogenase. *Science* **2017**, *16* (357), 928–932.

(18) Lorent, C.; Pelmenschikov, V.; Frielingsdorf, S.; Schoknecht, J.; Caserta, G.; Yoda, Y.; Wang, H.; Tamasaku, K.; Lenz, O.; Cramer, S. P.; Horch, M.; Lauterbach, L.; Zebger, I. Exploring Structure and Function of Redox Intermediates in [NiFe]-Hydrogenases by an Advanced Experimental Approach for Solvated, Lyophilized and Crystallized Metalloenzymes. *Angew. Chem. Int. Ed.* **2021**, *60* (29), 15854–15862.

(19) Bürstel, I.; Hummel, P.; Siebert, E.; Wisitruangsakul, N.; Zebger, I.; Friedrich, B.; Lenz, O. Probing the Origin of the Metabolic Precursor of the CO Ligand in the Catalytic Center of [NiFe] Hydrogenase. *J. Biol. Chem.* **2011**, *286* (52), 44937–44944.

(20) Lauterbach, L.; Wang, H.; Horch, M.; Gee, L. B.; Yoda, Y.; Tanaka, Y.; Zebger, I.; Lenz, O.; Cramer, S. P. Nuclear Resonance Vibrational Spectroscopy Reveals the FeS Cluster Composition and Active Site Vibrational Properties of an O_2-Tolerant NAD$^+$-Reducing [NiFe] Hydrogenase. *Chem. Sci.* **2015**, *6* (2), 1055–1060.

(21) Horch, M.; Schoknecht, J.; Wrathall, S. L. D.; Greetham, G. M.; Lenz, O.; Hunt, N. T. Understanding the Structure and Dynamics of Hydrogenases by Ultrafast and Two-Dimensional Infrared Spectroscopy. *Chem. Sci.* **2019**, *10* (39), 8981–8989.

(22) Dementin, S.; Burlat, B.; De Lacey, A. L.; Pardo, A.; Adryanczyk-Perrier, G.; Guigliarelli, B.; Fernandez, V. M.; Rousset, M. A Glutamate Is the Essential Proton Transfer Gate during the Catalytic Cycle of the [NiFe] Hydrogenase. *J. Biol. Chem.* **2004**, *279* (11), 10508–10513.

(23) Greene, B. L.; Vansuch, G. E.; Wu, C. H.; Adams, M. W. W.; Dyer, R. B. Glutamate Gated Proton-Coupled Electron Transfer Activity of a [NiFe]-Hydrogenase. *J. Am. Chem. Soc.* **2016**, *138* (39), 13013–13021.

(24) Evans, R. M.; Ash, P. A.; Beaton, S. E.; Brooke, E. J.; Vincent, K. A.; Carr, S. B.; Armstrong, F. A. Mechanistic Exploitation of a Self-Repairing, Blocked Proton Transfer Pathway in an O_2-Tolerant [NiFe]-Hydrogenase. *J. Am. Chem. Soc.* **2018**, *140* (32), 10208–10220.

(25) Tai, H.; Nishikawa, K.; Higuchi, Y.; Mao, Z.; Hirota, S. Cysteine SH and Glutamate COOH Contributions to [NiFe] Hydrogenase Proton Transfer Revealed by Highly Sensitive FTIR Spectroscopy. *Angew. Chem. Int. Ed.* **2019**, *131* (38), 13419–13424.

(26) Greene, B. L.; Vansuch, G. E.; Chica, B. C.; Adams, M. W. W.; Dyer, R. B. Applications of Photogating and Time Resolved Spectroscopy to Mechanistic Studies of Hydrogenases. *Acc. Chem. Res.* **2017**, *50* (11), 2718–2726.

(27) Ogata, H.; Nishikawa, K.; Lubitz, W. Hydrogens Detected by Subatomic Resolution Protein Crystallography in a [NiFe] Hydrogenase. *Nature* **2015**, *520* (7548), 571–574.

(28) Horch, M.; Lauterbach, L.; Mroginski, M. A.; Hildebrandt, P.; Lenz, O.; Zebger, I. Reversible Active Site Sulfoxygenation Can Explain the Oxygen Tolerance of a NAD$^+$-Reducing [NiFe] Hydrogenase and Its Unusual Infrared Spectroscopic Properties. *J. Am. Chem. Soc.* **2015**, *137*, 2555–2564.

(29) Horch, M.; Schoknecht, J.; Mroginski, M. A.; Lenz, O.; Hildebrandt, P.; Zebger, I. Resonance Raman Spectroscopy on [NiFe] Hydrogenase Provides Structural Insights into Catalytic Intermediates and Reactions. *J. Am. Chem. Soc.* **2014**, *136* (28), 9870–9873.

(30) Horch, M.; Rippers, Y.; Mroginski, M. A.; Hildebrandt, P.; Zebger, I. Combining Spectroscopy and Theory to Evaluate Structural Models of Metalloenzymes : A Case Study on the Soluble [NiFe] Hydrogenase from *Ralstonia eutropha*. *ChemPhysChem* **2013**, *14*, 185–191.

(31) Rippers, Y.; Horch, M.; Hildebrandt, P.; Zebger, I.; Mroginski, M. A. Revealing the Absolute Configuration of the CO and CN^- Ligands at the Active Site of a [NiFe] Hydrogenase. *ChemPhysChem* **2012**, *13* (17), 3852–3856.

(32) Happe, R. P.; Roseboom, W.; Egert, G.; Friedrich, C. G.; Massanz, C.; Friedrich, B.; Albracht, S. P. J. Unusual FTIR and EPR Properties of the H_2-Activating Site of the Cytoplasmic NAD-Reducing Hydrogenase from *Ralstonia eutropha*. *FEBS Lett.* **2000**, *466* (2–3), 259–263.

(33) Schneider, K.; Cammack, R.; Schlegel, H. G.; Hall, D. O. The Iron-Sulphur Centres of Soluble Hydrogenase from *Alcaligenes eutrophus*. *Biochim. Biophys. Acta - Protein Struct.* **1979**, *578* (2), 445–461.

(34) Germer, F.; Zebger, I.; Saggu, M.; Lendzian, F.; Schulz, R.; Appel, J. Overexpression, Isolation, and Spectroscopic Characterization of the Bidirectional [NiFe] Hydrogenase from *Synechocystis* Sp. PCC 6803. *J. Biol. Chem.* **2009**, *284* (52), 36462–36472.

(35) Schneider, K.; Cammack, R.; Schlegel, H. G. Content and Localization of FMN, Fe-S Clusters and Nickel in the NAD-linked Hydrogenase of *Nocardia opaca* 1b. *Eur. J. Biochem.* **1984**, *142* (1), 75–84.

(36) Zaborosch, C.; Köstert, M.; Bill, E.; Schneider, K.; Schlegel, H. G.; Trautweint, A. X. EPR and Mössbauer Spectroscopic Studies on the Tetrameric, NAD-Linked Hydrogenase of *Nocardia opaca* 1b and Its Two Dimers: 1. The Bδ-Dimer – a Prototype of a Simple Hydrogenase. *Biometals* **1995,** *8* (2), 149–162.

(37) Serebryakova, L. T.; Medina, M.; Zorin, N. A.; Gogotov, I. N.; Cammack, R. Reversible Hydrogenase of *Anabaena variabilis* ATCC 29413: Catalytic Properties and Characterization of Redox Centres. *FEBS Lett.* **1996**, *383* (1–2), 79–82.

(38) Van Der Linden, E.; Burgdorf, T.; De Lacey, A. L.; Buhrke, T.; Scholte, M.; Fernandez, V. M.; Friedrich, B.; Albracht, S. P. J. An Improved Purification Procedure for the Soluble [NiFe]-Hydrogenase of *Ralstonia eutropha*: New Insights into Its (in)Stability and Spectroscopic Properties. *J. Biol. Inorg. Chem.* **2006**, *11* (2), 247–260.

(39) Lubitz, W.; Ogata, H.; Ru, O.; Reijerse, E. Hydrogenases. Chem. Rev. **2014**, *114*, 4081–4148.

(40) Kraka, E.; Larsson, J. A.; Cremer, D. Generalization of the Badger Rule Based on the Use of Adiabatic Vibrational Modes. In Computational Spectroscopy: Methods, Experiments and Applications; Grunenberg, D. J., Ed.; Wiley-VCH Verlag GmbH & Co. KGaA, **2010**; 105–149.

(41) Ladd, J. A.; Orville-Thomas, W. J.; Cox, B. C. Molecular Parameters and Bond Structure-III. Carbon-Oxygen Bonds. *Spectrochim. Acta* **1964**, *20* (12), 1771–1780.

(42) Bruschi, M.; Tiberti, M.; Guerra, A.; De Gioia, L. Disclosure of Key Stereoelectronic Factors for Efficient H_2 Binding and Cleavage in the Active Site of [NiFe]-Hydrogenases. *J. Am. Chem. Soc.* **2014**, *136* (5), 1803–1814.

(43) Lauterbach, L.; Lenz, O. Catalytic Production of Hydrogen Peroxide and Water by Oxygen-Tolerant [NiFe]-Hydrogenase during H_2 Cycling in the Presence of O_2. *J. Am. Chem. Soc.* **2013**, *135*, 17897–17905.

(44) Winkler, M.; Duan, J.; Rutz, A.; Felbek, C.; Scholtysek, L.; Lampret, O.; Jaenecke, J.; Apfel, U. P.; Gilardi, G.; Valetti, F.; Fourmond, V.; Hofmann, E.; Léger, C.; Happe, T. A Safety Cap Protects

Hydrogenase from Oxygen Attack. *Nat. Commun.* **2021**, *12* (1), 1–10.

(45) Martins, M. C.; Romão, C. V; Folgosa, F.; Borges, P. T.; Frazão, C.; Teixeira, M. How Superoxide Reductases and Flavodiiron Proteins Combat Oxidative Stress in Anaerobes. *Free Radic. Biol. Med.* **2019**, *140*, 36–60.

(46) Sheng, Y.; Abreu, I. A.; Cabelli, D. E.; Maroney, M. J.; Miller, A. F.; Teixeira, M.; Valentine, J. S. Superoxide Dismutases and Superoxide Reductases. *Chem. Rev.* **2014**, 114 (7), 3854–3918.

(47) Pinto, A. F.; Rodrigues, J. V; Teixeira, M. Reductive Elimination of Superoxide: Structure and Mechanism of Superoxide Reductases. *Biochim. Biophys. Acta - Proteins Proteomics* **2010**, *1804* (2), 285–297.

(48) Horch, M.; Pinto, A. F.; Utesch, T.; Mroginski, M. A.; Romão, C. V.; Teixeira, M.; Hildebrandt, P.; Zebger, I. Reductive Activation and Structural Rearrangement in Superoxide Reductase: A Combined Infrared Spectroscopic and Computational Study. *Phys. Chem. Chem. Phys.* **2014**, *16* (27), 14220–14230.

(49) Berthomieu, C.; Dupeyrat, F.; Fontecave, M.; Verméglio, A.; Nivière, V. Redox-Dependent Structural Changes in the Superoxide Reductase from *Desulfoarculus baarsii* and *Treponema pallidum*: A FTIR Study. *Biochemistry* **2002**, *41* (32), 10360–10368.

(50) Yeh, A. P.; Hu, Y.; Jenney, F. E.; Adams, M. W. W.; Rees, D. C. Structures of the Superoxide Reductase from *Pyrococcus furiosus* in the Oxidized and Reduced States. *Biochemistry* **2000**, *39* (10), 2499–2508.

(51) Romao, C. V.; Matias, P. M.; Sousa, C. M.; Pinho, F. G.; Pinto, A. F.; Teixeira, M.; Bandeiras, T. M. Insights into the Structures of Superoxide Reductases from the Symbionts *Ignicoccus hospitalis* and *Nanoarchaeum equitans*. *Biochemistry* **2018**, *57* (36), 5271–5281.

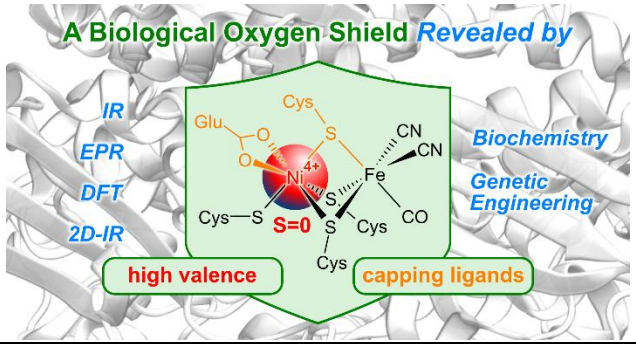
A Biological Oxygen Shield Revealed by
IR
EPR
DFT
2D-IR
Biochemistry
Genetic Engineering
Glu
Cys
Cys
Cys
Cys
CO
CN
CN
Fe
Ni
4+
S=0
high valence
capping ligands